Raman Lidar Measurements during the International H_20 Project. I. Instrumentation and Analysis Techniques – Popular Summary

D. N. Whiteman, B. Demoz, P. Di Girolamo, J. Comer, I. Veselovskii, K. Evans, Z. Wang, M. Cadirola, K. Rush, G. Schwemmer, B. Gentry, S. H. Melfi, B. Mielke, D. Venable, T. Van Hove

The amount of water vapor in the atmosphere helps to determine the likelihood that severe storms may develop. The concentration of water vapor, though, is highly variable in space and time. And yet small changes in water vapor concentration over a short period of time or over a short spatial distance can determine whether a storm may or may not develop. Therefore, in order to improve the ability to forecast severe weather such as thunderstorms it is important to measure water vapor in the atmosphere with high spatial and temporal resolution.

One of the most attractive research tools for measuring water vapor in the atmosphere with high spatial and temporal resolution is a Raman lidar. A Raman lidar consists of a laser transmitter, a telescope receiver and optics and electronics for processing optical and electronic signals. A laser pulse is emitted into the atmosphere and it interacts with molecules in the atmosphere causing them to become excited and to emit, through the Raman process, photons of different wavelength than emitted by the laser. The molecule that emitted these photons can be identified based on the wavelength of the photons emitted. This is the way that a Raman lidar identifies water vapor molecules in the atmosphere.

One of the great challenges in Raman lidar measurements has been to make useful daytime measurements of the water vapor profile under bright daytime conditions. In this first of two papers, we describe the instrumentation and analysis of the first documented Raman lidar that is able to measure water vapor in the daytime with sufficient quality to permit the study of developing storm systems.

Raman Lidar Measurements During the International H_2O Project. I. Instrumentation and Analysis Techniques

D. N. Whiteman, B. Demoz, P. Di Girolamo, J. Comer, I. Veselovskii, K. Evans, Z. Wang, M. Cadirola, K. Rush, G. Schwemmer, B. Gentry, S. H. Melfi, B. Mielke, D. Venable, T. Van Hove

To be submitted to Journal of Atmospheric and Oceanic Technology

Abstract

The NASA/GSFC Scanning Raman Lidar (SRL) participated in the International H_2O Project (IHOP) that occurred in May and June, 2002 in the Midwestern part of the U. S. The SRL received extensive optical modifications prior to and during the IHOP campaign that added new measurement capabilities and enabled unprecedented daytime water vapor measurements by a Raman Lidar system. Improvements were also realized in nighttime upper tropospheric water vapor measurements. The other new measurements that were added to the SRL for the IHOP deployment included rotational Raman temperature, depolarization, cloud liquid water and cirrus cloud ice water content. In this first of two parts, the details of the operational configuration of the SRL during IHOP are provided along with a description of the analysis and calibration procedures for water vapor mixing ratio, aerosol depolarization and cirrus cloud extinction to backscatter ratio. For the first time, a Raman water vapor lidar calibration is performed taking full account of the temperature sensitivity of Raman water vapor and nitrogen scattering. Part two presents case studies that permit the daytime and nighttime error statistics to be quantified.

1 Table Of Contents

2 Introduction

The International H_2O Project was the largest meteorological field campaign ever held in the United States [Wechworth et. al., 2004]. It occurred in the mid-western United States between May 13 - June 25, 2002. The goal of IHOP was to measure convective storm systems with sufficient detail to permit quantitative precipitation and convection initiation forecasting to be improved. During IHOP, numerous intensive operations periods were declared focussing on boundary layer evolution, drylines, bores, nocturnal jets, and other mesoscale events. IHOP included participants from numerous U.S. and foreign government agencies as well as universities.

The instrumentation used during IHOP included seven research aircraft carrying three water vapor lidars and one wind lidar, mobile radar systems for storm-chasing, and a ground-based site in the western panhandle of Oklahoma that included the NASA/Goddard Space Flight Center (GSFC) Scanning Raman Lidar (SRL), Goddard Laboratory for Winds (GLOW) molecular wind lidar [Gentry et. al., 2004], and the Holographic Airborne Rotating Lidar Instrument Experiment (HARLIE) [Schwemmer et. al., 2004] scanning aerosol lidar. Other instruments that were located at the western Oklahoma site that came to be known as "Homestead" were Vaisala RS-80 G15H and SnowWhite radiosonde systems [Wang et. al., 2003], cloud and aerosol radar, sodar, Atmospheric Emitted Radiance Interferometer (AERI) [Feltz et. al., 1998], SuomiNet Global Positioning System (GPS) [Ware et. al., 2000] and an Aerosol Robotic Network (AERONET) [Holben et. al., 1998] sun photometer.

This first of two papers provides a detailed description of the experimental configuration of the NASA/GSFC SRL during its participation in IHOP. This configuration included measurements of water vapor mixing ra-

tio, aerosol backscatter, extinction and depolarization, rotational Raman temperature measurements performed in the UV [Di Girolamo et. al., 2004], cloud liquid water [Russo et. al, 2004], and cirrus cloud particle size and ice water content [Wang et. al., 2004]. All of these measurements were made using a single output wavelength of 354.7 nm demonstrating the feasibility of providing these measurements in an automated and eye-safe system [Di Girolamo et. al., 2004]. Particular attention will be given here to the instrumentation and analysis techniques that led to improved daytime water vapor measurement capability. With these improvements, it is now possible to use a single experimental configuration for quantifying water vapor variation in the boundary layer during the daytime and extending into the upper troposphere at night. The paper is structured as follows. A brief history of the use of the narrow-band, narrow field-of-view technique for Raman water vapor lidar measurements is provided as context for the SRL water vapor measurements in IHOP. The techniques for processing the raw data and of calculating water vapor mixing ratio, aerosol scattering ratio, aerosol depolarization and cirrus cloud extinction to backscatter ratio are then presented. In part two of this paper, comparisons of the SRL water vapor measurements with those of other instruments at IHOP will be presented along with daytime and nighttime case studies that demonstrate measurement capability and permit the error statistics to be quantified.

3 The Pursuit of Non-Solar Blind Daytime Raman Water Vapor Lidar Measurements

During IHOP, the SRL demonstrated greatly improved non-solar-blind daytime Raman water vapor lidar measurements over any previously demonstrated. The combination of technologies and techniques that permitted this were 1) a large-pulse tripled Nd:YAG laser, 2) narrow field of view telescope, 3) narrow spectral

band detection, 4) fast photomultiplier detectors and 5) a combination of analog and photon counting electronics, which permit the full intensity Raman signals to be sampled. While none of these elements is new, the combination had not been fully exploited previously for Raman water vapor lidar. Furthermore, the path toward this solution was not direct and occurred over more than 20 years of research activity at various research centers.

3.1 The first efforts in Raman water vapor lidar at NASA/GSFC

The first Raman water vapor lidar measurements were made nearly simultaneously in 1969 in separate research efforts by S. H. Melfi [Melfi et. al., 1969] and J. Cooney [Cooney, 1970]. Development of Raman lidar technology for measurement of water vapor was started at NASA/GSFC in 1980 when Dr. Melfi joined the center. The first Raman water vapor lidar system developed at GSFC was based on a QuantaRay DCR1-A tripled Nd:YAG laser (354.7 nm) operating at 10 Hz and providing 150 mj per pulse in the UV. The laser had a single, flash-lamp pumped, amplifier and used harmonic crystals for converting the 1.064 μm fundamental wavelength to the doubled and tripled wavelengths of 532 nm and 354.7 nm, respectively. The crystal housings were not temperature stabilized necessitating tilt-tuning of the crystals to maximize the output energy every two minutes during extended data acquisition periods. The telescope used was based on a 1.5 m searchlight mirror that was built in Japan and used on a German surface ship in World War II. The mirror was found in a military equipment storage facility at Chesapeake Beach, Virginia, moved to GSFC, re-coated and placed into service for use in Raman lidar. A Cassagrain configuration telescope was constructed using this mirror so that the detector package could be installed under the very large telescope. The telescope had relatively poor optical quality so that the received signals were measured

using a field of view of 2-5 milliradians. Furthermore, due to uncertainty about whether the substrate material had been annealed, no hole was cut in the mirror so that the return signal were transmitted through the uncoated substrate. A simple detector package consisting of beamsplitters, interference filters and two photomultiplier tubes measuring the Raman signals from water vapor (407.5 nm) and nitrogen (386.7 nm) was used. The interference filters were manufactured by Barr Associates and possessed approximately 15-20% transmission with bandwidths of 5-10 nm. The data system used LeCroy 8837F 8-bit, 32-MHz analog-to-digital (AD) transient recorders and was controlled by a Digital Equipment Computer PDP-11 running the RT-11 operating system. This system was known as the Marine Boundary Layer Raman Water Vapor Lidar and was successfully used to chart the evolution of water vapor in the boundary layer in 1985 [Melfi and Whiteman, 1985]. The system was housed in a mobile trailer and was first used in a field deployment for the Cooperative Huntsville Meteorological Experiment (COHMEX) in Huntsville, Alabama in 1986 [Dodge et. al., 1986] [Fulton and Heymsfield, 1991] [Straka and Anderson, 1993].

The nighttime limitation of this early Raman water vapor lidar system was clear but there was no real progress toward the development of daytime Raman water vapor lidar measurements at GSFC throughout the 1980s despite the fact that the solar blind technique of making daytime Raman water vapor measurements was being demonstrated successfully by others [Renault and Capitini, 1988]. During the 1980s, upgrades to the Marine Boundary Layer Raman Water Vapor Lidar included replacing the searchlight-based telescope with an astronomical quality, 0.75 m aperture system and implementing dual photomultiplier detection channels in a low altitude/high altitude configuration for water vapor, nitrogen and Rayleigh-Mie measurements. The new telescope, although possessing just 1/4 of the collecting area of the former one,

significantly improved the signal-to-noise ratio of the measurements due to the greatly reduced losses (both scattering and transmission) and improved focussing quality. The data acquisition system was also upgraded to add photon counting (PC) electronics (Joerger S3 200 MHz counters) to the pre-existing analog detectors. The first published measurements of water vapor and aerosol structure of cold and warm frontal passages were made using this system [Melfi et. al., 1989], although the measurements were still limited to nighttime.

By the late 1980s, most of the necessary technology was in place to attempt a non-solar blind measurement of daytime water vapor except that interference filter technology still did not permit the fabrication of the high transmission, narrow bandwidth optics that are now available. Furthermore, frequent ground loop and impedance matching problems associated with the simultaneous use of AD and PC measurements encouraged testing the idea of using photon counting electronics exclusively as a replacement for the combined AD and PC system that was in use previously. Two photomultipliers tubes, both operating in the photon counting mode, were used for each measured wavelength. The near range channel was attenuated significantly to permit it to be photon-counted while the far-range channel received the full intensity signal. This concept produced excellent measurements during nighttime tests performed using the Marine Boundary Layer Water Vapor Lidar in 1987. Due to funding limitations in the late 1980s, development work on Raman lidar at GSFC ceased for a period of time and this mobile Raman water vapor lidar was converted into the first mobile stratospheric ozone lidar: STROZ-LITE (Stratospheric Ozone Lidar Trailer Experiment) [McGee et. al., 1991].

3.2 Early Non-Solar Blind Daytime Raman Water Vapor Lidar Activities

The first published measurements of daytime water vapor mixing ratio using non-solar blind Raman lidar were performed in 1991 in northern Germany [Ansmann et. al., 1992] using the narrow field-of-view, narrow spectral band technique being discussed here. The measurements were made using a high power XeCl laser (>67.5W), 300 MHz photon counting electronics, 0.8 m telescope operating at 0.1 - 0.4 milliradian field-of-view, and grating polychromator providing approximately 0.3 nm bandpass. An additional edge filter was used in the water vapor channel to increase the suppression of the Rayleigh-Mie signal. Due to the low optical efficiency of the system, no attenuation of the signal was required during daytime measurements to permit the signal to be recorded using only photon counting electronics (private communication, Drs. Albert Ansmann and Ulla Wandinger). Measurements with 10-50% random error were made with this system to an altitude of ~1.7 km using 15 minutes averaging, and ~200 m spatial smoothing.

The need within the atmospheric radiation community to improve the measurements of water vapor and other parameters to support atmospheric radiative transfer modeling led to technology development within the U.S. Department of Energy (DOE) of water vapor measurement systems with improved accuracy and precision [Goldsmith et. al., 1998]. The DOE Instrument Development Program (IDP) began in 1989 and provided partial funding for the development of the first implementation of the NASA/GSFC Scanning Raman Lidar (SRL). This work was carried out jointly between NASA/GSFC and DOE Sandia National Laboratory (SNL) in a research effort that resulted in the construction of two Raman lidar systems: one at GSFC and the other at SNL. The systems shared the same telescopes and used excimer lasers, but key aspects of the designs were different to explore multiple techniques for making daytime Raman water vapor

lidar measurements. The NASA/GSFC effort pursued the solar-blind approach for daytime water vapor measurements and therefore used a fluorine-optimized excimer laser that could operate using either a XeF (351 nm for nighttime measurements) or a KrF (248 nm for daytime measurements) gas mixture. The SNL effort used the narrow-band, narrow field of view approach [Bisson et. al., 1999] and was based on a XeCl laser providing 40-50W of output power. This parallel development effort resulted in the first side-by-side demonstration of Raman water vapor lidar measurements in 1994 [Goldsmith et.al., 1994]. The SNL system later demonstrated the concept of using a large aperture telescope at narrow field of view for improved daytime measurements [Bisson et. al., 1999] and helped to demonstrate some of the concepts that were designed into the CART Raman Lidar, the first automated Raman lidar system [Goldsmith et. al., 1998].

The success of this technology demonstration effort led to the development of a new Raman lidar at the DOE Southern Great Plains (SGP) site in northern Oklahoma [Goldsmith et. al., 1998]. That system, referred to now as CARL (Climate Research Facility Raman Lidar), became operational in 1996 and uses a Nd:YAG laser operating at 9-12W and the narrow-band, narrow-field-of-view approach. CARL's original configuration used only photon counting data acquisition thus requiring aq factor of 10 attenuation of the Raman signals during the daytime to prevent photon saturation. Nonetheless, with a 10-minute average and 75-meter range resolution, water vapor mixing ratio measurements with less than 20% random error to an altitude of approximately 3 km were performed. Several years of such measurements are now available, providing continuous measurements of water vapor throughout the diurnal cycle [Turner and Goldsmith, 1999]. In June of 2004, the data acquisition system of CARL was upgraded to include both analog and photon counting electronics essentially identical to those in use in the SRL for IHOP permitting the full strength

Raman signals to be used during both daytime and nighttime [?].

4 The Scanning Raman Lidar (SRL)

Development of the NASA/GSFC Scanning Raman Lidar began in 1989 under the support of both NASA and DOE's IDP Program. The SRL was first deployed in the field in November 1991 for the Spectral Radiance Experiment [Ellingson and Wiscombe, 1996] that was sponsored by NASA and DOE and took place in Coffeyville, Kansas. At that time the system was based on a Lambda Physik LPX 240iCC excimer laser that produced up to 30 watts at 351 nm using a XeF gas mixture and up to 100 Watts at 248 nm using a KrF gas mixture. Nighttime measurements were performed using the 351 nm output of the laser and daytime measurements [Whiteman et. al., 1994] were made using the 248 nm output and the solar blind technique [Renault and Capitini, 1988] whereby solar background is essentially eliminated by absorption due to stratospheric ozone. The use of the solar blind technique requires a knowledge of the tropospheric ozone profile so that the differential extinction of the H_2O and N_2 signals by ozone can be accounted for in the water mixing ratio calculation. This approach to Raman water vapor measurements permitted photon counting data acquisition (100 MHz in the initial implementation of the SRL) to be used exclusively. The solar blind measurements of water vapor using the SRL were hampered by the large attenuation of the outgoing laser radiation due to tropospheric ozone which caused signal-induced-noise (SIN) problems in the PMT detectors in use at the time. The PMTs were upgraded in 1993 to ones with significantly lower SIN problems, but still overlap problems prevented an accurate quantification of the ozone profile in the lowest 1 km [Whiteman et. al., 1994]. Also, the absorption cross section of ozone does not differ greatly between the Raman-shifted returns for N_2 and O_2 when excited by 248 nm [Goldsmith and Ferrare, 1994]

[Whiteman et. al., 1994]. This degrades the sensitivity of the technique for deriving ozone. Theoretical modeling [Goldsmith and Ferrare, 1994] indicates that a longer excitation wavelength of approximately 260nm would be greatly preferred for solar blind measurements. Nonetheless, daytime solar blind water vapor mixing ratio measurements were made with the SRL in 1993 to an altitude of 2.5 km using a 20 minute average [Whiteman et. al., 1994].

The narrow spectral band, narrow field-of-view technique for making Raman water vapor lidar measurements was also explored with the SRL in 1992 using the XeF (351 nm) output of the excimer laser. These measurements were performed by expanding the laser beam by a factor of 5 and using a 0.5 milliradian field of view. However, the 100-MHz photon counting data acquisition system, fully sufficient for the original solar-blind conception of the SRL, was incapable of handling the high countrates present in non-solar blind daytime Raman lidar measurements. Thus, the input signals required attenuation by more than 2 orders of magnitude to permit them to be photon-counted. Nonetheless, daytime measurements were performed through the boundary layer with 1 hour averaging [Whiteman et. al., 1994]. In the early 1990's therefore we had determined that addition of analog electronics would be necessary to optimize daytime measurements using the narrow-band, narrow-field-of-view technique.

It was also clear that, considering a fixed amount of output power, a smaller number of larger laser pulses offered significant advantages for daytime operations [Bisson et. al., 1999] over a larger number of smaller pulses. Therefore, in 1995, a Nd:YAG laser was added to the SRL in preparation for the TARFOX (Tropospheric Aerosol Radiation Field Observational Experiment) field campaign [Ferrare et. al., 2000]. Narrow spectral band, narrow field-of-view measurements of water vapor were performed using the SRL

during TARFOX and can be seen at our website (http://ramanlidar.gsfc.nasa.gov), however the 100-MHz photon counting data system was still in use requiring that the input signals be attenuated by at least an order of magnitude in order to limit the photon arrival rate. In addition, the interference filters available at the time were limited to approximately 25% transmission for a 0.5 nm passband.

4.1 Additional technology development and the SRL configuration for IHOP

Drawing on the previous experience gained in Raman water vapor lidar development, in 1998 we began construction of the Raman Airborne Spectroscopic Lidar (RASL) under the NASA Instrument Incubator Program (IIP). The goal of this instrument was to bring the range of Raman lidar water vapor and aerosol measurements to an airborne platform and to take advantage of performance enhancements that are realized by measuring downward in the atmosphere versus measuring upward [Whiteman et. al., 2001b]. This new development effort included the purchase of a new data acquisition system from Licel of Berlin, Germany that incorporates both analog and photon counting electronics and that circumvented one of the limitations of the earlier daytime Raman water vapor lidar measurements. The RASL data acquisition system was used in the SRL for the IHOP field deployment. By the time of IHOP, significantly improved interference filters were also available for Raman water vapor measurements. These two enhancements were critical to the successful water vapor measurements made by the SRL during IHOP.

Many additional modifications were made to the SRL immediately prior to and during the IHOP field campaign. Substantially new wavelength separation optics were implemented on the large 0.76m F/5.2 Dall-Kirkham telescope. This provided simultaneous measurements of water vapor mixing ratio, aerosol backscatter and extinction, cloud liquid [Whiteman and Melfi, 1999] [Russo et. al, 2004] and ice water

[Wang et. al., 2004], and rotational Raman temperature [Di Girolamo et. al., 2004]. In addition, a 0.25m F/2.5 Newtonian telescope was added in the field during the IHOP experiment for the low altitude Raman measurements, accomplished via fiber optic coupling, and for aerosol depolarization measurements using free-space coupled optics. The fiber-coupled measurements from this telescope were not useful during IHOP due to an improperly coated mirror. Because of this problem, most data products were processed to a minimum altitude of 300 meters; the lowest altitude to which the data from the large telescope were useful. The laser used was the same laser that was installed in the SRL prior to the TARFOX field campaign: a Continuum tripled Nd:YAG laser operating at 354.7 nm operating at 30 Hz and generating approximately 9 W of output power. The fields of view of the large and small telescopes were approximately 0.3 and 1.2 mrad, respectively. The narrow field-of-view of the large telescope coupled with narrow spectral filters in the water vapor and nitrogen channels (2.5A and 2.8A, respectively) and the combined use of analog and photon counting data acquisition permitted the full intensity water vapor and nitrogen signals to be sensed throughout the diurnal cycle with no instrumental changes occurring during the measurements. The previous configuration of both the SRL and CARL required attenuation filters during the daytime due to the high solar background. The addition of analog data acquisition electronics and narrow spectral bandpass filters now permits the full intensity signal to be sampled diurnally. This enabled the water vapor mixing ratio to be quantified during the daytime at significantly higher temporal and spatial resolution than was previously possible. Table 1 shows the specifications of the SRL during IHOP and notes the components/measurements that were new for IHOP.

NASA/GSFC Scanning Raman Lidar Specifications for the IHOP field campaign		
Component	Description	Notes
Laser	Continuum Custom longcavity Nd:YAG tripled. 30 Hz, 300 mj/pulse	converted to closely emulate model 9030
Telescope (high altitude)	Starr Optical, Dall-Kirkham, 0.76 m, F/5.2 horizontally mounted	variable FOV, but nominally 0.3 milli-radians
Telescope (low altitude)	Custom Newtonian, 0.25 m, F2.5	1.2 milliradian field of view. New for IHOP.
Spectrum Analyzer	Custom designed using Barr dichroic beamsplitters and interference filters	
Measurement/ Filter - Large telescope		
Rotational Raman (352/1.2 nm)		new for IHOP
Rotational Raman (354/0.3 nm)		new for IHOP
Rayliegh-Mie (354.7/0.3 nm)		
Raman Nitrogen (386.7/0.3 nm)		
Raman Liquid/Ice water (403/6.0 nm)		new for IHOP
Raman water vapor (407.6/0.25 nm)	now tilt-tuned to center at 407.48 nm	
Measurement/ Filter - Small telescope		
Rayleigh-Mie (354.7/0.3 nm)	fiber coupled	new for IHOP
Perpendicular polarization (354.7/0.3 nm)	direct coupled	new for IHOP
Parallel polarization (354.7/0.3 nm)	direct coupled	new for IHOP
Raman nitrogen (386.7/0.3 nm)	fiber coupled	new for IHOP
Raman liquid/ice water (403/6.0 nm)	fiber coupled	new for IHOP
Raman water vapor (407.65/0.25 nm)	now tilt-tuned to center at 407.48 nm	new for IHOP
Scanning Mirror	Starr Optical, 1.1m x 0.8m flat, 50mm thickness	
Scan Motor Assembly	Custom twin-axle, belt-drive design with 22-bit shaft encoder	
PMTs	Hamamatsu R1924 (selected for high gain, high blue sensitivity and low dark counts) and R7400	
PMT Housings	Products for Research	
Data Acquisition System	Licel Analog + Photon Counting Transient Recorders (7.5m spatial resolution)	
Data Acquisition Computer	PC running Windows 2000	

Table 1: Hardware and optical configuration of the NASA/GSFC Scanning Raman Lidar during the IHOP field campaign

5 Data Analysis Techniques

Numerous atmospheric quantities were measured by the SRL during IHOP as shown in Table 1. For all of these measurements, the first step in the analysis is combining the AD and PC data into a single composite profile for each signal measured. That procedure will now be described.

5.1 Combined Analog and Photon Counting Data - "Gluing"

The Licel data acquisition electronics in use in the SRL measure a lidar signal simultaneously using 20 MHz, 12-bit analog to digital converters and 250 MHz photon counters. Two separate data streams are maintained within the instruments that must be merged in some fashion to create a final output profile for each channel. The process of combining the analog and photon counting data together has come to be known as "gluing". After experimenting with various methods of calculating the conversion between an analog voltage and a photon countrate, the following procedure was used to determine mean conversion factors that are used to convert the analog data to a "virtual" countrate scale.

The photon counting data are first corrected for photon pulse pile-up assuming the photon counting circuitry behaves in a non-paralyzable fashion [Whiteman et. al., 1992] [Whiteman et. al., 2003a]. The background is subtracted separately from the analog and photon counting records. Then, ordered pairs of analog and photon counting data are formed in a region of the signal where both are considered to be responding linearly and that avoids problem areas such as near the time when the laser fires. The low and high countrate thresholds that define this region are typically 1 and 10-20 MHz, respectively, for our Hamamatsu 1924 PMTs that possess a pulse width of 4-5 ns. The points in the profile that fall within these ranges and satisfy the other conditions are then formed as ordered pairs and a linear regression is performed on these points.

As an additional noise filter, the residuals between the actual data points and the best fit linear regression are then calculated and any points outside of 2 standard deviations from the mean are excluded. For the Rayleigh-Mie channels, additional noise filtering using 95% quantile regression was sometimes required. This regression technique is illustrated in the upper and middle plots of figure 1. In the upper plot, the regression of the analog and photon counting ordered pairs is shown with and without the application of the photon pulse pile-up correction. The slope (in MHz/mV) and offset (in MHz) of the regressions are given in the figure. Notice that the regression of the pulse pile-up corrected data exhibits a slope approximately 10% higher than the uncorrected data. Also, the offset of the corrected data is much closer to zero. The middle plot of the figure is a blowup of the portion of the regression near the origin to permit the offsets to be seen more clearly. Since the background has already been subtracted separately from the analog and photon counting data, the value of the optimum resolving time can be determined by studying the offset versus the resolving time used in the pile-up correction. The optimum resolving time is the one that yields an offset closest to zero. This technique can be contrasted with what was done previously to determine the optimum resolving time using purely photon counting systems [Whiteman et. al., 1992] [Whiteman et. al., 2003a] where a significantly attenuated version of the signal was used as the linear signal instead of the analog signal as used here. The technique illustrated here should be valid as long as the non-paralyzable equation properly describes the counting behavior of the electronics and the analog electronics are providing linear measurements. The non-paralyzable equation is certainly just an approximation of the counting behavior of the electronics so it is important to limit the maximum countrate of the data used to determine the optimum value of the resolving time. The analysis of the offset versus resolving time shown in the lower panel of

figure 1, performed using a countrate range of 1-20 MHz, shows that ~5 ns is the optimum value. For comparison, the RMS differences between the non-paralyzable model and the actual data points are also shown as a function of resolving time. There is a poorly defined minimum at approximately 2 ns. We do not consider this determination of the resolving time to be reliable due to the very shallow minimum in the RMS curve. The minimum becomes better defined using this technique if higher countrates are permitted in the regression. However, considering that the non-paralyzable correction already amounts to ~11% at 20 MHz using 5 ns for the resolving time, determining the optimum resolving time using higher countrates will be more subject to errors introduced by the assumption that the electronics behave in a purely non-paralyzable fashion. Therefore, we choose to determine the optimum resolving time based on the zero crossing for the offset.

5.1.1 Gluing coefficients and water vapor mixing ratio calibration

Variations in the Raman lidar water vapor mixing ratio calibration can have important consequences for meteorological application of Raman lidar measurements. Therefore, it is important to study the behavior of the analog to photon counting conversion factors under differing conditions. In particular, the behavior of the slopes of the regressions as the background is increasing due to increased solar radiation is of particular interest. Data acquired on June 19-20, 2002 will now be used to illustrate the gluing process.

The times series of fully calibrated water vapor mixing ratio is presented in figure 2a. As will be discussed in section 5.2, the water vapor mixing ratio calculation is performed using the Raman water vapor and nitrogen measurements. Figures 2b and 2c therefore show which portions of the fully processed water vapor image shown in a) used AD (shown in white) and PC (black) data from the water vapor and nitro-

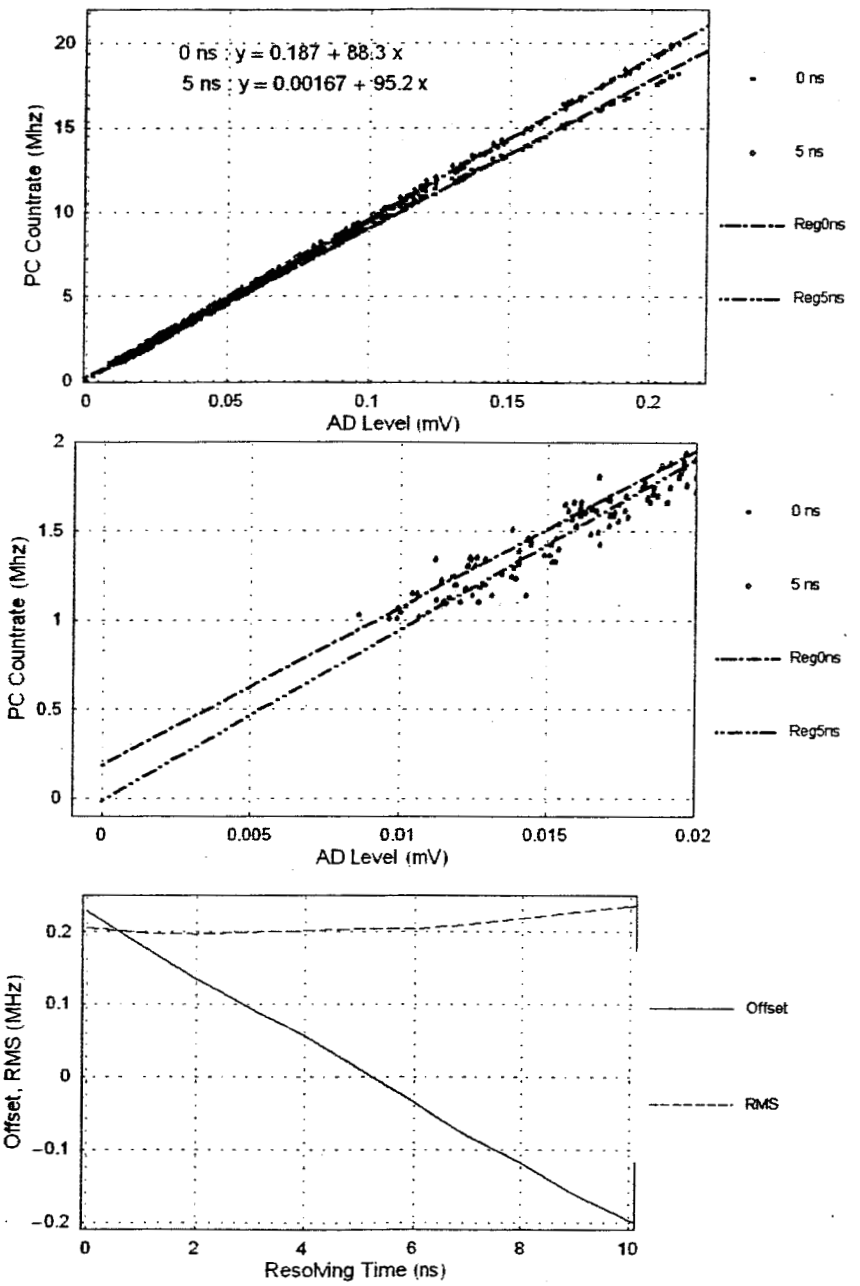

Figure 1: Upper: two regressions of {analog, photon couting} data pairs are shown: before and after the correction for pulse pile up. Middle: the same data as in the upper plot but a blow up near the origin to show the intercept values more clearly. Lower: calculated offset of the linear regression versus resolving time value. The optimum resolving time of ~5 ns produces a near-zero offset. For comparison, the RMS of the residuals for each regression are also shown. This method of determining the optimum resolving time is less sensitive than the offset approach.

gen signals. One can see that for daytime measurements only analog data were used whereas during the nighttime a combination of AD and PC are used. It is during the periods of reduced solar background when the gluing process can be used in the Raman channels. A time series of the gluing conversion factors is therefore presented in figure 2d for both the water vapor signal and the nitrogen signals where a transition period between daytime and nighttime measurements has been chosen. At the beginning of the period shown, mean photon counting signals exceed 20 MHz and therefore a regression between AD and PC data was not performed. At approximately 0150 UTC (indicated as 2550 in the figure), the solar background decreased to the point where it was possible to perform the regression. But as the figure shows, the regressions that occur during the transition from day to night are characterized by low correlation coefficients (R^2 multiplied by 10) and significantly changing slopes. Through experimentation, it was determined that good quality regressions resulted if the mean background countrate was below the minimum threshold frequency set to be 1 MHz in this example. The time at which this occurred (~2610 UTC) is indicated by the vertical line in the figure. The calculated slopes and correlation coefficients (R^2) tend to decrease quickly to the left of this line, which defines the region where the background points qualify for the regression. To the right of this line the mean H_2O (indicated by $m(H_2O)$) and N_2 ($m(N_2)$) slopes are ~$8.4 \pm 0.08 \times 10^{10}$ and $9.5 \pm 0.03 \times 10^{10} Hz/Volt$ ($10^{10} Hz/Volt = 10\ MHz/mV$), respectively. The N_2 slope is quite constant beyond the transition point but, even though the variation in the H_2O slope beyond the transition point is less than 1%, the slight tendency for the H_2O slope to increase with time is still under investigation.

Even though good quality regressions are obtained under most circumstances using the technique just described, the profile to profile conversion factor between AD and PC is subject to statistical fluctuations

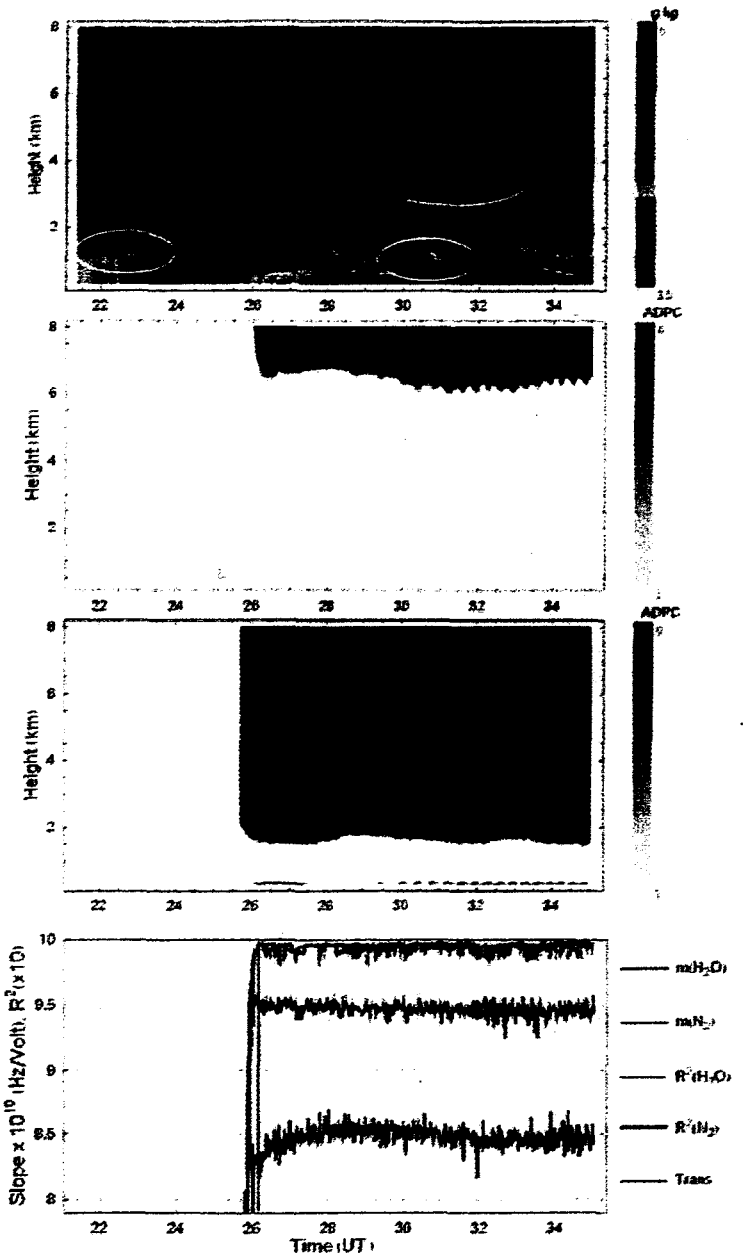

Figure 2: First panel: water vapor mixing ratio variation during the period of June 19-20, 2002 in IHOP. Three wave regions are encircled. The major bore event was at ~30.5 UT and 0.5 km. Second panel: diagram indicating the use of either analog (white) or photon counting data (black) for the nitrogen data used in calculating the water vapor mixing shown in the top panel. Third panel: diagram indicating the use of either analog (white) or photon counting data (black) for the water vapor data used in calculating the water vapor mixing shown in the top panel. Fourth panel: time series of slopes of the regressions used to determine the coefficients to convert analog data to a virtual photon counting scale.

that likely do not reflect variation in the gain of the electronics. Therefore, it is desirable to use a single conversion factor for each channel for an entire data record. For the IHOP data processing, the mean values of the conversion factors obtained for a portion of nighttime data were thus used to glue the AD and PC data for those parts of the profile where the countrate exceeded 20 MHz. When the mean values of the PC background exceeded 1 MHz (e.g. prior to 2610 UTC in figure 2), the AD data (converted to countrate using the conversion factors) were used exclusively without gluing.

5.2 Water vapor mixing ratio calculation

The water vapor mixing ratio is defined as the mass of water vapor divided by the mass of dry air in a given volume. It is conserved in atmospheric processes that do not involve condensation or evaporation and thus serves as a tracer for air parcels. Also, the vertical profile of mixing ratio strongly influences atmospheric stability. Water vapor mixing ratio can be calculated using the following expression [Whiteman et. al., 2003b] by taking the ratio of the Raman water vapor (407.5 nm) and nitrogen signals (386.7 nm) and accounting for the atmospheric differential transmission that occurs at the two different return wavelengths.

$$w = k\frac{O_N(r)}{O_H(r)}\frac{F_N(T)}{F_H(T)}\frac{P(\lambda_H, r)}{P(\lambda_N, r)}\frac{\frac{d\sigma_N(\pi)}{d\Omega}}{\frac{d\sigma_H(\pi)}{d\Omega}}\frac{\xi(\lambda_N)}{\xi(\lambda_H)}\Delta\tau(\lambda_N, \lambda_H, r) \quad (1)$$

$$k \cong 0.78\frac{MW_{H_2O}}{MW_{DryAir}} \cong 0.485 \quad (2)$$

where w is the water vapor mixing ratio typically expressed in units of g kg^{-1}, $O_N(r)/O_H(r)$ is the ratio of overlap functions for the N_2 (N) and H_2O (H) channels, k is a proportionality constant determined by the ratio of molecular weights of water (MW_{H_2O}) and dry air (MW_{DryAir}) and the fraction of air comprised by molecular nitrogen (~0.78), $F_N(T)/F_H(T)$ is the ratio of the temperature dependent functions for the

Raman N_2 and H_2O channels, where for example $F_H(T)$ is defined by

$$F_H(T) = \frac{\int_{\Delta\lambda_H} \frac{d\sigma_H(\lambda',\pi,T)}{d\Omega}\, \xi\left(\lambda'\right)\, d\lambda'}{\frac{d\sigma_H(\pi)}{d\Omega}\, \xi\left(\lambda_H\right)} \tag{3}$$

$F_H(T)$ carries all the temperature dependence of the lidar equation for the water vapor channel. It contains the effects of any changes in the system transmission efficiency, $\xi(\lambda)$, for wavelengths other than λ_H within the passband $\Delta\lambda_H$. $\xi(\lambda_H)$ is the transmission efficiency at λ_H. The notation $d\sigma_H(\pi)/d\Omega$ is used to indicate the total Raman backscatter cross section for water vapor at the stimulating wavelength. The product $F_H(T)\frac{d\sigma_H(\pi)}{d\Omega}$ may be viewed as the effective molecular cross section that is consistent with the use of a monochromatic optical efficiency term, $\xi(\lambda_H)$, in equation 1. $P(\lambda_X, r) = S(\lambda_X, r) - B(\lambda_X, r)$, where $P(\lambda_X, r)$ is the background subtracted power in the Raman channel for species X, and S and B represent the signal and background, respectively. Thus, $P(\lambda_H, r)/P(\lambda_N, r)$ is the ratio of background-subtracted signals from the H_2O and N_2 channels, $\frac{d\sigma_N(\pi)}{d\Omega}/\frac{d\sigma_H(\pi)}{d\Omega}$ is the ratio of the full Raman cross sections for N_2 and H_2O, $\xi(\lambda_N)/\xi(\lambda_H)$ is the ratio of N_2 and H_2O lidar channel efficiencies at their characteristic wavelengths of λ_N and λ_H and $\Delta\tau(\lambda_H, \lambda_N, r)$ is the differential atmospheric transmission that occurs at the Raman shifted wavelengths λ_N and λ_H. The value of $\Delta\tau$ is determined from:

$$\Delta\tau(\lambda_H, \lambda_N, r) = \exp\left(-\int_0^r \{\alpha(\lambda_H, r') - \alpha(\lambda_N, r')\} dr'\right) \tag{4}$$

where r is the range to the volume of interest, and α is the extinction coefficient (units of inverse length).

The equations used to quantify the random error in the water vapor mixing ratio, assuming Poisson statistics, are given below.

$$\frac{\sigma^2_{R_w}}{R^2_w} = \frac{\sigma^2_{SH} + \sigma^2_{BH}}{(S_H - B_H)^2} + \frac{\sigma^2_{SN} + \sigma^2_{BN}}{(S_N - B_N)^2} \quad (5)$$

$$\sigma^2_{R_w} = \frac{(S_H - B_H)^2}{(S_N - B_N)^2}\left(\frac{\sigma^2_{SH} + \sigma^2_{BH}}{(S_H - B_H)^2} + \frac{\sigma^2_{SN} + \sigma^2_{BN}}{(S_N - B_N)^2}\right) \quad (6)$$

In these equations, R_w represents the ratio of the background-subtracted water vapor and nitrogen lidar signals. In other words, $R_w = (S_H - B_H) / (S_N - B_N)$, where S_X and B_X are shorthand for $S(\lambda_X, r)$ and $B(\lambda_X, r)$, respectively [Whiteman et. al., 2003b].

5.2.1 Overlap correction for the water vapor mixing ratio measurement

Simple geometrical ray trace considerations indicate that in calculating a quantity from a ratio of two lidar channels that use a common field stop (such as the water vapor and nitrogen signals used in calculating the water vapor mixing ratio given by equation 1), the overlap functions $O_N(r)$ and $O_H(r)$ are equal and thus cancel. In real applications, however, this ratio does not equal unity in the near field and a residual overlap function must be determined and applied as a correction to the data. The existence of a residual overlap function appears to be due to the fact that as laser light propagates from the near field to the far field of the telescope, light received by the optical detection system spreads across optical components such as interference filters and photomultiplier tubes that may possess position-dependent efficiencies. These effects are greatest in the near field where modern radiosondes can provide high quality measurements of relative humidity, temperature and pressure. For the IHOP analysis, therefore, a mean residual overlap correction function was calculated by using 26 comparisons of SRL and Vaisala RS-80 radiosonde profiles of water vapor mixing ratio that occured during IHOP. The mean residual overlap correction function resulting from that calculation was then applied to all IHOP water vapor mixing ratio data as a part of the data reduction.

The residual overlap correction function was unity above an altitude of 750 meters and decreased to 0.94 at an altitude of 300 meters, the minimum altitude of processed data for IHOP. Therefore the maximum correction produced by this residual overlap correction function was 6%.

5.2.2 Temperature dependence of Raman scattering

The temperature dependence of narrowband water vapor and nitrogen Raman measurements was also accounted for in the analysis of the IHOP water vapor mixing ratio data. An analysis of the temperature dependence of Raman water vapor and nitrogen scattering and its influence on the mixing ratio calculation indicates that 1) the effect is dominated by the temperature dependence of the water vapor spectrum and not the N_2 spectrum and 2) the net effect for likely filter configurations is to yield an apparent excess in water vapor concentrations that tends to increase with altitude [Whiteman et. al., 2003a] [Whiteman et. al., 2003b]. This latter effect is due primarily to a shift of intensity in the Raman spectrum of water vapor toward the band origin as temperatures decrease with altitude.

To assess the magnitude of this effect for the IHOP measurements, laser output and interference filter transmission properties were carefully measured in order to apply the results of the earlier theoretical studies. The Continuum laser frequency-doubled wavelength was measured using a Burleigh 4500 wavemeter and found to be 532.07 +/- 0.005 nm. Assuming errors are random and uncorrelated, this implies a frequency tripled wavelength of 354.71 +/- 0.003 nm. In addition, the water vapor and nitrogen interference filter bandpass characteristics were measured using a Thermo-Electron Nicolet 870 Fourier Transform Spectrometer (FTS) operating at 0.5 cm^{-1} resolution. The spectrometer was calibrated using a mercury lamp since the internal calibration based on a Helium Neon (HeNe) laser was found to not be reliable for measure-

ments in the near UV region of the spectrum (i.e. at shorter wavelengths than the HeNe calibration source). The combined error of the FTS measurement and mercury calibration did not exceed 0.001 nm. Figure 3 shows the mercury lamp calibration corrected measurements of the water vapor interference filter transmission overlaid on the Raman scattering spectrum of water vapor calculated at $270K$ using the data from reference [Avila et. al., 1999]. The figure shows that the peak of the water vapor interference filter used for the IHOP water vapor measurements was shifted long of the peak in the Raman water vapor spectrum by approximately 0.05 nm. (Our comparison of traditional grating spectrometer measurements of filter central position and those obtained with the mercury lamp calibrated FTS instrument have revealed consistent differences in center line position of between 0.02 - 0.05 nm. The FTS measurements are considered more reliable due to the instrument's inherent linear response, the repeatability of the mercury calibration of the FTS and, in a grating spectrometer, the difficulty of accounting for the sinusoidal variation of spectral position between calibration points.) The fact that the filter was positioned long of the peak of the water vapor spectrum introduced considerable temperature sensitivity to the measurement of water vapor over the range of temperatures present in the troposphere as will be shown later. It should be mentioned here that tilting the filter so as to operate at a shorter wavelength such as 407.45 would essentially eliminate the temperature dependence of water vapor with altitude. Since the time of the IHOP field campaign, this tilt-tuning has been implemented in the SRL.

A study of the transmission properties of the SRL indicated that all significant variation in the lidar system efficiency over the passband of the Raman water vapor feature was confined to the water vapor interference filter itself. Therefore, the filter transmission measurements versus wavelength can be used

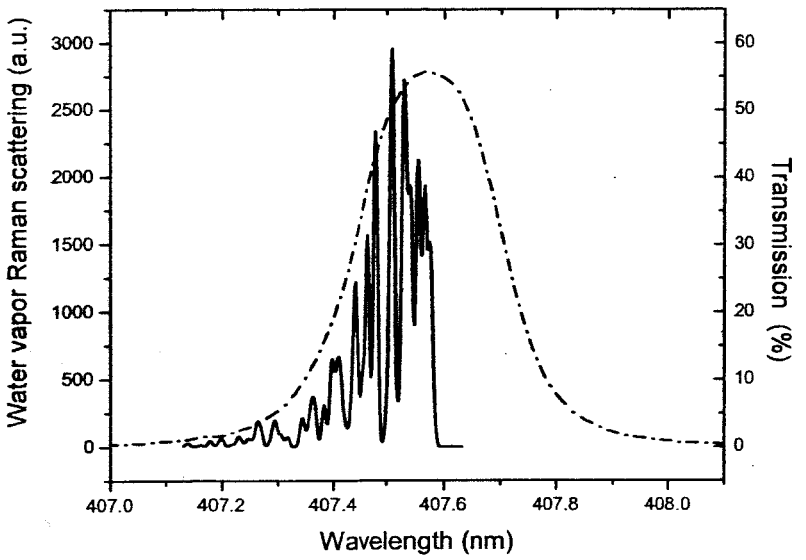

Figure 3: Water vapor interference filter transmission measurements using a mercury-lamp calibrated Fourier Transform Spectrometer operating at 0.5 cm^{-1} resolution. For reference, the Raman water vapor spectrum simulated at 270K is also plotted. The shift in the filter from the peak of the Raman spectrum implies significant temperature sensitivity for the water vapor measurement.

to indicate the variation of the lidar system efficiency over the water vapor passband. Similar analysis of the Raman nitrogen measurements were made and combined to generate the mean temperature correction vector, $F_N[T(r)]/F_H[T(r)]$ from equation 1, that was applied to all the SRL water vapor mixing ratio profiles during the reduction of the IHOP data. This correction vector is shown in figure 4. The mean IHOP temperature correction vector varies by approximately 10% from the surface to an altitude of 14 km. This implies that, for the configuration of the SRL during IHOP, the correction to the water vapor mixing ratio due the temperature dependence of Raman scattering is approximately 10% in the troposphere. For comparison, the temperature correction vector calculated for the same filter characteristics but assuming the U.S. Standard Atmosphere temperature profile is also shown. As this comparison implies, the residual error due to using a single temperature correction vector for all of the IHOP data is estimated to be 1% or less. The temperature correction vector for the same set of water vapor and nitrogen filters, but if the water vapor filter had been tilt-tuned to 407.45 nm, is also shown in the figure. Notice that for a filter position of 407.45 nm, the values of the ratio $F_N[T(r)]/F_H[T(r)]$ are lower for this nearly temperature insensitive configuration indicating that a larger fraction of the Raman water vapor cross section is being transmitted. Figure 4 demonstrates that for the configuration of IHOP a significant temperature- (and thus altitude-) dependent correction was required for the water vapor mixing ratio calculation. However, the figure also shows that, even for a narrow water vapor interference filter such as used in the SRL for IHOP (2.5 Å), the temperature sensitivity can essentially be eliminated with proper tuning of system parameters if accurate measurements of laser output wavelength and lidar system transmission characteristics are available.

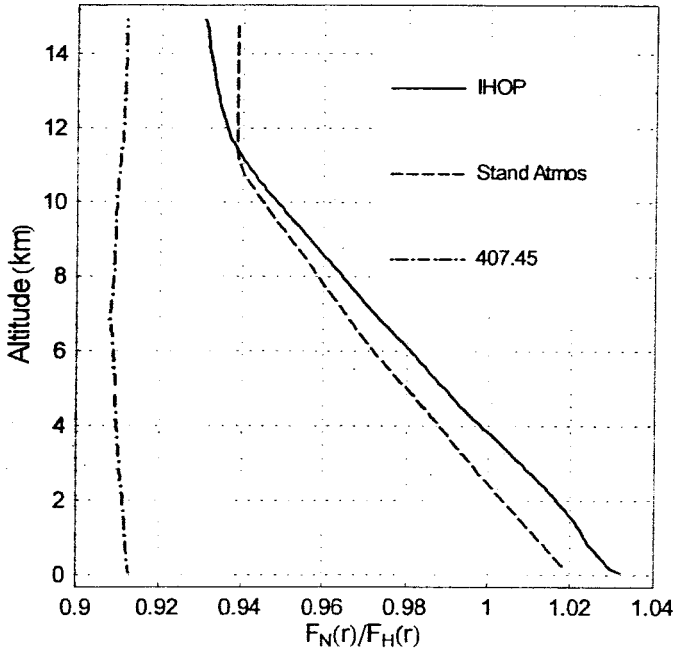

Figure 4: Temperature correction vectors $F_N[T(r)]/F_H[T(r)]$ for the water vapor mixing ratio calculation. The vector applied during the IHOP analysis is shown along with the vector corresonding to the U.S. Standard Atmosphere assuming the same experimental configuration as in IHOP. The curve laveled 407.45 is the temperature vector that would result if the water vapor filter had been positioned at 407.45 nm through tilt tuning. This latter configuration is nearly temperature insensitive throughout the troposphere.

5.2.3 Water vapor mixing ratio calibration

A first principles Raman water vapor lidar calibration can be performed with standard optical laboratory procedures. However, the ratio of the Raman cross sections for water vapor and nitrogen is not known to better than 10%, which implies that the absolute accuracy of such an effort will exceed 10% [Vaughan et. al., 1988] [Sherlock et. al., 1999]. Calibration by comparison with other water vapor sensors, such as research grade radiosonde, microwave radiometer or GPS, is thus the standard within the Raman water vapor lidar community and the general technique that was used to calibrate the SRL water vapor measurements during IHOP.

In particular, the SRL water vapor mixing ratio measurements during IHOP were calibrated by comparing the integral of the lidar mixing ratio profile with the total precipitable water (PW) derived from a SuomiNet GPS [Ware et. al., 2000] system mounted on the SRL. During the daytime, the SRL water vapor profile extended usefully only to the top of the boundary layer, thus leaving a significant fraction of the total precipitable water unmeasured. Therefore to calculate PW from the lidar during the daytime, SRL calibrations with respect to GPS were limited to radiosonde launch times and the radiosonde profile was normalized to the lidar and used to extend the lidar mixing ratio profile upward beyond the point at which 25% random error was present in the lidar data. To account for the portion of the mixing ratio profile near the ground not measured by the lidar, a linear interpolation was performed between the lowest altitude measured by the lidar (typically 300m) to the ground point measured by a Paroscientific Met3A station associated with the SuomiNet GPS system. This composite profile was then integrated to yield the SRL total precipitable water for daytime comparisons with GPS. For nighttime comparisons, it was not necessary to

extend the profile upward using radiosonde since the lidar water vapor data were of sufficient quality to permit ~99% of the PW to be quantified based on standard atmosphere concentrations of water vapor above the maximum lidar height measured. However, the downward extension to the ground was still necessary.

Except for three dates during IHOP (June 14, 17, 18), the water vapor data were processed using a single, height independent calibration constant determined from the GPS calibration procedure just described. On these days, the lidar calibration differed by 10-15% from the mean calibration value perhaps due to accidental changes in system operating parameters such as PMT high voltage. For these cases the calibration constant used was the one determined on that day instead of the mean value. The standard deviation of the calibration constant for the IHOP water vapor mixing ratio data, including the effects of these anomalous days, was approximately 6%. When using only daytime measurements it was approximately 6.5% and 4.5% when using only nighttime measurements. The smaller standard deviation of the calibration constant for nighttime measurements is thought to be due to greater atmospheric horizontal homogeneity at night and thus the better agreement between the profile of water vapor measured over the lidar site and the volume average measurement of the GPS. The daytime and nighttime calibration constants agreed to within ~1% implying that there was no significant difference in the lidar water vapor calibration constant due to diurnal effects.

GPS as the calibration source for Raman water vapor lidar The U. S. DOE Atmospheric Radiation Measurements (ARM) program calibrates its Raman lidar, CARL, in a similar fashion as just described for the SRL except that the CARL PW is compared to the total column water vapor measured by microwave radiometer [Turner et. al., 2002]. Research done within the DOE ARM program indicates that carefully

calibrated and analyzed microwave radiometer (MWR) data possess an absolute accuracy of approximately 3-4%. This makes it an excellent calibration standard for atmospheric research. A deployment of the SRL to the DOE Southern Great Plains site in Oklahoma in 2003 for the AIRS Water Vapor Experiment-Ground (AWEX-G) [?] permitted a careful comparison of the ARM microwave radiometer and the same SuomiNet GPS system that accompanied the SRL into the field for IHOP.The GPS measures over a much larger volume than the MWR and therefore individual comparisons can show considerable disagreement under conditions of spatial non-homogeneity in the atmosphere. Line of site comparisons of the two instruments have been performed to address these differences and have shown excellent agreement [Braun et. al., 2003]. During AWEX-G, we performed an extended comparison of 30-minute average GPS and MWR vertical precipitable water measurements in order to minimize the effects of short term spatial inhomogeneities. The results of that comparison are shown in figure 5.

The plot on the left of the figure shows that the slope of the regression between GPS and MWR was essentially unity but, due to an offset of ~0.4 mm, the PW from GPS was on average 2.4% higher than MWR. This overall agreement of the two sensors is within the uncertainty of the MWR, supporting the use of the GPS system as an independent source for calibration. The plot on the right of figure 5 presents the comparison of MWR and GPS PW hour by hour. The overall moist bias of the GPS with respect to MWR that was indicated by the regression can be seen throughout the diurnal period. However, the GPS shows a slight tendency to become moister during the daytime period from ~1200 - 2400 UTC. The source of this small diurnal bias is under investigation but it is not thought to be due to variations in the MWR since comparisons of AERI and MWR scaled radiosondes have indicated no significant diurnal bias in the MWR

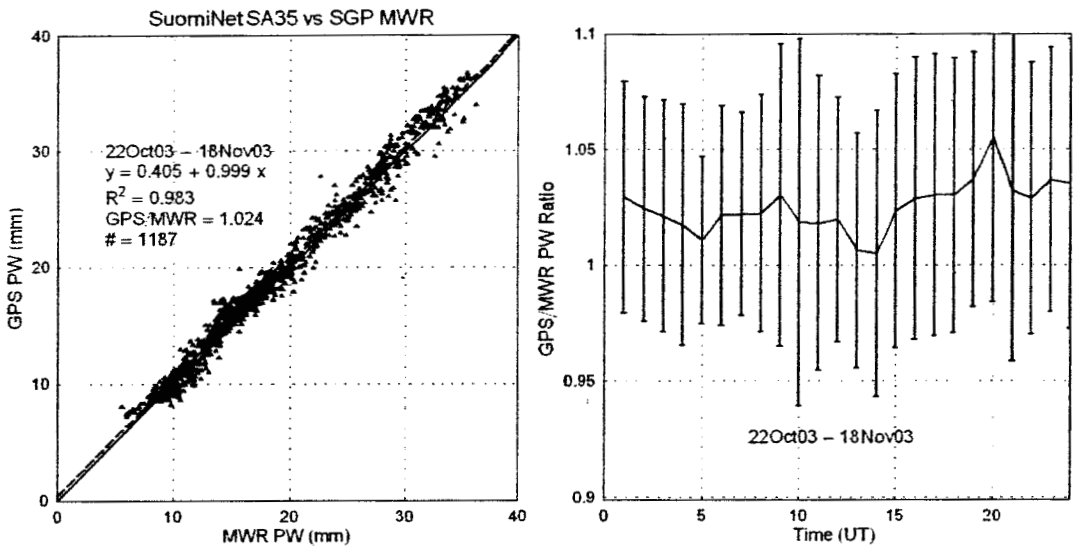

Figure 5: Left: An analysis of the precipitable water measurements from the SuomiNet GPS that accompanied the SRL to IHOP and served as the source of the water vapor calibration and the U.S. DOE microwave radiometer at their Southern Great Plains research site. There is a mean offset of ~2.4% which is within the absolute uncertainty of the MWR. The best fit regression is shown with a dashed line. The solid line indicates perfect 1-1 correlation. Right: The same data as plotted on the left except this time divided by time of day. A small diurnal bias between GPS and MWR is observed.

[Turner et. al., 2002]. This analysis indicates that the GPS calibration agrees well with the DOE MWR and offers similar absolute accuracy as a source for Raman water vapor lidar calibration provided sufficient statistics are accumulated to reduce the effects of spatial non-homogeneities in the atmosphere.

5.3 Aerosol scattering ratio and backscatter coefficient

The aerosol scattering ratio, $\mathcal{R}$, is defined as the ratio of the total (molecular and particle) backscatter coefficient divided by the molecular backscatter coefficient. It can be calculated from the ratio of the received power in the Rayleigh-Mie and Raman vibrational N_2 channels. The equations for calculating the aerosol scattering ratio, including the effects of the temperature dependence of rotational and vibrational scattering are [Whiteman et. al., 2003b]

$$\mathcal{R}(\lambda_L, r) - 1 = C_N^*(\lambda_L, r) F_N(T(r)) \frac{P(\Delta\lambda_R, r)}{P(\Delta\lambda_N, r)} \Delta\tau(\lambda_N, \lambda_L, r) - F_R(T(r)) \quad (7)$$

$$C_N^*(\lambda_L, r) = C_N(\lambda_L) \frac{O_N(r)}{O_R(r)} \frac{\xi(\lambda_N)}{\xi(\lambda_L)} \quad (8)$$

$$C_N(\lambda_L = 355) \simeq 0.78 \frac{d\sigma_N(\pi)/d\Omega(\lambda_L = 355)}{d\sigma_{mol}(\pi)/d\Omega(\lambda_L = 355)} \simeq 0.78 \frac{2.8 \times 10^{-30}}{3.2 \times 10^{-27}} \simeq 6.8 \times 10^{-4} \quad (9)$$

where $P(\Delta\lambda_R, r)$ and $P(\Delta\lambda_N, r)$ are the background-subtracted received power in the channels measuring the Rayleigh-Mie signal in the spectral band $\Delta\lambda_R$ and the vibrational N_2 Raman-shifted in the spectral band $\Delta\lambda_N$. The differential transmission, $\Delta\tau(\lambda_N, \lambda_L, r)$, is the ratio of atmospheric transmission at the two wavelengths, λ_N and λ_L and is calculated using an equation similar to 4. The lidar channel optical efficiencies are expressed as $\xi(\lambda_N)$ and $\xi(\lambda_L)$. The lidar system overlap functions are given by $O_N(r)$ and $O_R(r)$. The calibration constant C_N has been evaluated at the laser wavelength of ~355 nm using the values of the Raman vibrational and Rayleigh differential scattering cross-sections, $d\sigma_N(\pi)/d\Omega$ and $d\sigma_{mol}(\pi)/d\Omega$, respectively [Measures 1984]. The effect of the temperature dependence of the Raman

scattering on the Rayleigh-Mie and Raman nitrogen signals is contained in the two terms, $F_R(T(r))$ and $F_N(T(r))$, respectively, which are calculated using an equation similar to 3. The aerosol backscatter coefficient, $\beta^{aer}(\lambda_L, r)$, can be evaluated from the aerosol scattering ratio as follows

$$\beta^{aer}(\lambda_L, r) = \beta_\pi^{mol}(\lambda_L, r)\left(\mathcal{R}(\lambda_L, r) - 1\right)$$

where $\beta_\pi^{mol}(\lambda_L, z)$ is the Rayleigh backscatter coefficient at the laser wavelength calculated using density measurements from a radiosonde.

5.4 Cirrus cloud optical depth and layer mean extinction to backscatter ratio

Cirrus cloud optical depth can be calculated from a Raman lidar measurement of molecular nitrogen, which, if properly performed, shows only attenuation due to the presence of the cloud. The amount of this attenuation can be converted to optical depth once the atmospheric density is known. The single scattering equation which yields two-way optical depth is obtained by integrating the equation for aerosol extinction [Whiteman et. al., 2003a] and can be written as:

$$\begin{aligned}
&\int_{r_1}^{r_2} \left[\alpha(\lambda_L, r) + \alpha(\lambda_N, r)\right]\, dr \\
&= \ln\left(\frac{O_N(r_2)\, F_N(T(r_2))\, N_N(r_2)\, r_1^2\, P(\lambda_N, r_1)}{O_N(r_1)\, F_N(T(r_1))\, N_N(r_1)\, r_2^2\, P(\lambda_N, r_2)}\right) - \int_{r_1}^{r_2} \left[\alpha_{mol}(\lambda_L, r) + \alpha_{mol}(\lambda_N, r)\right]\, dr \\
&\approx \ln\left(\frac{N_N(r_2)\, r_1^2\, P(\lambda_N, r_1)}{N_N(r_1)\, r_2^2\, P(\lambda_N, r_2)}\right) - \int_{r_1}^{r_2} \left[\alpha_{mol}(\lambda_L, r) + \alpha_{mol}(\lambda_N, r)\right]\, dr
\end{aligned} \tag{10}$$

where r_1 is below the cloud, r_2 is above the cloud, λ_L is the laser wavelength (354.7 nm), λ_N is the wavelength of the Raman nitrogen signal (386.7 nm), $\alpha(\lambda_x, r)$ is the cloud extinction coefficient as a function of wavelength and range, $O_N(r)$ is the overlap function for the nitrogen channel evaluated at

range r, $F_N(T(r))$ is the temperature dependent factor for the Raman nitrogen measurement, $N_N(r)$ is the number density of atmospheric nitrogen (using the full atmospheric number density yields equivalent results) as a function of range, $P(\lambda_N, r)$ is the background-subtracted Raman lidar nitrogen signal and $\alpha_{mol}(\lambda_x, r)$ is the extinction coefficient due to molecular scattering obtained from radiosonde data. At typical cirrus altitudes, the ratios of the overlap and temperature dependent factors are nearly unity and can be ignored as shown in the final form of equation 10, which is the same result that would be obtained by integrating the traditional aerosol extinction equation [Ansmann et. al., 1992]. Assuming no multiple scattering and that cirrus cloud extinction is wavelength insensitive between λ_L and λ_N, the optical depth of the cloud is simply one-half of equation 10.

A modified approach to the evaluation of equation 10 was used here which implements an iterative procedure that corrects for the influence of multiple scattering [Whiteman et. al., 2001a] using a Gaussian approximation technique [Eloranta, 1998] and calculates a layer mean particle radius in the process. The integrated backscatter is determined by integrating the profile of cirrus cloud backscatter coefficient, which has been shown to be essentially insensitive to multiple scattering [Wandinger, 1998]. The layer mean extinction to backscatter ratio, also known as the lidar ratio, is then just the ratio of the cloud optical depth and the integrated backscatter coefficient.

5.5 Aerosol depolarization

The ability to calculate scattering ratios using the Raman lidar technique permits both the volume and

particle depolarization ratios δ_{vol} and δ_{par} to be calculated [Behrendt and Nakamura, 2002] as follows.

$$\delta_{vol}(z) = \frac{\beta_{\perp}^{mol}(z)+\beta_{\perp}^{par}(z)}{\beta_{\parallel}^{mol}(z)+\beta_{\parallel}^{par}(z)} = \frac{R_{\perp}(z)}{R_{\parallel}(z)}\delta_{mol}(z) \quad (11)$$

$$\delta_{par}(z) = \frac{\beta_{\perp}^{par}(z)}{\beta_{\parallel}^{par}(z)} = \frac{R_{\perp}(z)-1}{R_{\parallel}(z)-1}\delta_{mol}(z) \quad (12)$$

where β refers to the backscatter coefficients for either molecules (mol) or particles (par) in either the perpendicular ($\perp$) or parallel ($\parallel$) directions. $R_{\perp}$ is the scattering ratio for the perpendicular polarization signal and $R_{\parallel}$ is the scattering ratio for the parallel polarized signal. The equation for the scattering ratio used here is given in 7 and fully accounts for both the temperature dependence of Raman scattering as described in section 5.3.

The aerosol depolarization measurements were calibrated by first determining the relative gain of the parallel and perpendicular channels by observing a fully depolarized source, in this case thick overcast skies. Using this value of the relative gain in the channels, the volume depolarization ratio in clear air was found to be ~1.7% as opposed to the theoretical value of molecular depolarization of ~0.5% that corresponds to our ~0.5A bandpass filters. The additional depolarization was attributed to misalignment between the planes of polarization of the outgoing laser and the polarization analyzer [Reichardt et. al., 2003]. In order to compensate for the resulting cross-talk between the parallel and perpendicular channels, an approximate correction technique was used here. The volume depolarization ratio was calculated assuming variable amounts of cross talk between the parallel and perpendicular channels. The amount of assumed cross talk that yielded the theoretical value of 0.5% depolarization in clear air was used to analyze the depolarization data presented in part II. This amount of cross talk corresponded to an angular difference of ~3 degrees between the laser polarization and the position of the polarization analyzer. Another correction that was

applied to the depolarization data was to account for the variation in the molecular depolarization as a function of temperature [Behrendt and Nakamura, 2002]. The value of molecular depolarization for the filters in use and the range of temperatures observed during IHOP was found to vary as a function of temperature from approximately 0.46 - 0.52%.

6 Summary

The NASA/GSFC participated in the first International H_2O Project in May-June 2002. A new configuration of the SRL enabled measurements of water vapor, aerosol backscatter, extinction, depolarization, liquid water, ice water and rotational Raman temperature. In particular the combination of narrow field of view, narrow spectral bandpass, relatively large pulse energy Nd:YAG laser and both analog and photon counting detection electronics permitted a single configuration to be used for both daytime and nighttime measurements of water vapor mixing ratio. The improved water vapor measurement capability permits convective boundary layer processes to be studied throughout the diurnal cycle. In this first of two parts, the method of joining the analog and photon counting data, referred to as "gluing", was described for the case of water vapor measurements during a period that included a large number of atmospheric waves. For the first time, the temperature dependence of Raman scattering was accounted for in the calibration of a Raman water vapor and aerosol lidar and shown, for the configuration of the SRL during IHOP, to effect the upper tropospheric water vapor measurements by approximately 10%. A study of the calibration of water vapor mixing ratio indicated a stable calibration constant to within 1% between daytime and nighttime measurements. The measurements presented here were all provided using a single output wavelength of 354.7 nm demonstrating the feasibility of offering all of these measurements in an automated, eye-safe Raman lidar

system. In part two [Whiteman et. al., 2005b], comparisons of SRL measurements with other sensors are presented along with daytime and nighttime case studies.

7 Acknowledgements

The authors would like to thank the NASA Interdisciplinary Program managed by Dr. Jim Dodge for its support of this activity.

8 References

[Ansmann et. al., 1992] Ansmann, A., M. Riebesell, U. Wandinger, C. Weitkamp, E. Voss, W. Lhamann, W. Michaelis, 1992: Combined Raman Elastic-Backscatter LIDAR for Vertical Profiling of Moisture, Aerosol Extinction, Backscatter and LIDAR Ratio, Appl. Phys. B, B55, 18-28.

[Avila et. al., 1999] Avila, G., J. M. Fernandez, B. Mate, G. Tejeda, S. Montero, 1999: Ro-vibrational Raman Cross Sections of Water Vapor in the OH Stretching Region, *J. Mol. Spectr.*, **196**, 77-92.

[Behrendt and Nakamura, 2002] Behrendt A., T. Nakamura, 2002: Calculation of the calibration constant of polarization lidar and its dependency on atmospheric temperature, OPTICS EXPRESS, 10 (16): 805-817.

[Bisson et. al., 1999] Bisson, S. E., J. E. M. Goldsmith, M. G. Mitchell, 1999: Narrow-band, narrow-field-of-view Raman lidar with combined day and night capability for tropospheric water-vapor profile measurements, *Appl. Opt.*, Vol. 38, No. 9, 1841-1849.

[Braun et. al., 2003] Braun J, Rocken C, Liljegren J, 2003: Comparisons of line-of-sight water vapor observations using the global positioning system and a pointing microwave radiometer, J. Atmos. Ocean. Tech. 20 (5): 606-612.

[Cooney, 1970] Cooney, J., 1970: Remote Measurements of Atmospheric Water Vapor Profiles Using the Raman Component of Laser Backscatter, *J. Appl. Meteor.*, **9**, 182-184.

[Di Girolamo et. al., 2004] Di Girolamo, P., R. Marchese, D. N. Whiteman, B. B. Demoz, 2004: Rotational Raman Lidar measurements of atmospheric temperature in the UV, Geophys. Res. Lett., 31, L01106, doi:10.1029/2003GL018342.

[Dodge et. al., 1986] Dodge, J., J. Arnold, G. Wilson, Evans J. Fujita T., 1986: The Cooperative Huntsville Meteorological Experiment (COHMEX), Bull. Amer. Meteor. Soc., 67 (4): 417-419.

[Ellingson and Wiscombe, 1996] Ellingson R. G. , W. J. Wiscombe, 1996: The spectral radiance experiment (SPECTRE): Project description and sample results, Bull. Amer. Meteor. Soc. 77 (9): 1967-1985.

[Eloranta, 1998] Eloranta, E. W., 1998: Practical model for the calculation of multiply scattered lidar returns, *Appl. Opt.*, **37**,12, 2464-2472.

[Feltz et. al., 1998] Feltz, Wayne F., William L. Smith, Robert O. Knuteson, Henry E. Revercomb, Harold M. Woolf, and H. Ben Howell, 1998: Meteorological applications of temperature and water vapor retrievals from the ground-based Atmospheric Emitted Radiance Interferometer (AERI). *J. of*

Appl. Meteor., 37, 857-875.

[Ferrare et. al., 2000] Ferrare, R., S. Ismail, E. Browell, V. Brackett, M. Clayton, S. Kooi, S.H. Melfi, D.Whiteman, G. Schwemmer, K. Evans, P. Russell, J. Livingston, B. Schmid, B. Holben,L. Remer, A. Smirnov, and P. Hobbs, 2000: Comparison of aerosol optical properties and water vapor among ground and airborne lidars and sunphotometers during TARFOX, J. of Geophys. Res., 105, No. D8, 997-9933.

[Fulton and Heymsfield, 1991] Fulton, R., G. Heymsfield, 1991: Microphysical and Radiative Characteristics of Convective Clouds during COHMEX, J. Appl. Meteor.30 (1): 98-116.

[Gentry et. al., 2004] Gentry, B., 2004: GLOW Measurements during IHOP, Proceedings, 22nd International Laser Radar Conference, Matera, Proceedings, SP-561 ESA Ed., Volume I, 2004, ISBN 92-9092-872-7.

[Goldsmith and Ferrare, 1994] Goldsmith, J.E.M., R. A. Ferrare, Performance modeling of daytime Raman lidar systems for profiling atmospheric water vapor", in Sixteenth International Laser Radar Conference, M. P. McCormick, ed., NASA Conf. Pub. 3158 (NASA, Washington, D.C., 1992), Pt. 2, pp. 667-670.

[Goldsmith et.al., 1994] Goldsmith, J.E.M., S.E. Bisson, R.A. Ferrare, K.D. Evans, D.N. Whiteman, S.H. Melfi, 1994: Raman Lidar Profiling of Atmospheric Water Vapor: Simultaneous Measurements with Two Colocated Systems, Bull. Amer. Meteor. Soc., 75, No. 6, 975-982.

[Goldsmith et. al., 1998] Goldsmith JEM, Blair FH, Bisson SE, Turner DD, 1998: Turn-key Raman lidar for profiling atmospheric water vapor, clouds, and aerosols APPLIED OPTICS 37 (21): 4979-4990.

[Holben et. al., 1998] Holben BN, Eck TF, Slutsker I, Tanre D, Buis JP, Setzer A, Vermote E, Reagan JA, Kaufman YJ, Nakajima T, 1998: Lavenu F, Jankowiak I, Smirnov A, "AERONET - A federated instrument network and data archive for aerosol characterization", Remote Sens. Env. 66 (1): 1-16.

[Measures 1984] R. M. Measures, *Laser Remote Sensing Fundamentals and Applications*, (Wiley-Interscience, New York, New York, 1984).

[McGee et. al., 1991] McGee, T. J., D. Whiteman, R. Ferrare, J. J. Butler and J. Burris, 1991: "STROZ LITE: NASA Goddard Stratospheric Ozone Lidar Trailer Experiment", Opt. Eng. Vol 30, No. 1.

[Melfi et. al., 1969] Melfi, S. H., J. D. Lawrence, Jr., M. P. McCormick, 1969: Observation of Raman Scattering by Water Vapor in the Atmosphere, *App. Phys. Lett.*, **15**, 295.

[Melfi and Whiteman, 1985] Melfi, S. H.., and D. Whiteman, 1985: Observation of Lower-Atmospheric Moisture Structure and its Evolution using a Raman Lidar, Bull. Amer. Meteor. Soc. 66 1288-1292.

[Melfi et. al., 1989] Melfi, S. H., D. N. Whiteman, R. A. Ferrare, 1989: Observation of atmospheric fronts using Raman lidar moisture measurements, *J. App. Meteor.*, **28**, 789-806.

[Reichardt et. al., 2003] Reichardt, J, R. Baumgart, T. J. McGee, 2003: Three-signal method for accurate measurements of depolarization ratio with lidar, *Appl. Opt.*, 42, 24, 4909-4913.

[Renault and Capitini, 1988] Renault, D., R. Capitini, 1988: Boundary Layer Water Vapor Probing with a Solar-Blind Raman Lidar: Validations, Meteorological Observations and Prospects, *J. Atmos. Ocean. Tech.*, Vol. 5, No. 5.

[Russo et. al, 2004] Russo, F, D. N. Whiteman, B. Demoz, Z. Wang, I. Veselovskii, R. Hoff, Development of Raman Lidar Techniques to address the Aerosol Indirect Effect: The Liquid Water Content of Clouds, Proceedings, 22nd International Laser Radar Conference, Matera, Proceedings, SP-561 ESA Ed., Volume I, 2004, ISBN 92-9092-872-7.

[Schwemmer et. al., 2004] Schwemmer, G., HARLIE Measurements during IHOP, Proceedings, 22nd International Laser Radar Conference, Matera, Proceedings, SP-561 ESA Ed., Volume I, 2004, ISBN 92-9092-872-7.

[Senff et. al., 1994] Senff, C., J. Bösenberg, G. Peters, 1994: Mesurement of water-vapor flux profiles in the convective boundary-layer with lidar and RADAR-RASS, J. Atmos. Ocean. Tech., 11 (1): 85-93.

[Straka and Anderson, 1993] Straka, J. M., J. Anderson, 1993: Numerical Simulations of microburst-producing storms - Some Results Observed during COHMEX, J. Atmos. Sci., 50 (10): 1329-1348.

[Sherlock et. al., 1999] Sherlock, V., A. Hauchecorne, J. Lenoble, 1999: Methodology for the independent calibration of Raman backscatter water-vapor lidar systems, *App. Opt.*, **38**, 27, 5816-5837.

[Turner and Goldsmith, 1999] Turner D.D., J. Goldsmith, 1999: Twenty-four-hour Raman lidar water vapor measurements during the Atmospheric radiation Measurement program's 1996 and 1997 water vapor intensive observation periods, J. Atmos. Ocean. Tech. 16 (8): 1062-1076.

[Turner et. al., 2002] Turner DD, Ferrare RA, Brasseur LAH, Feltz WF, 2002: Automated retrievals of water vapor and aerosol profiles from an operational Raman lidar, J. Atmos. Ocean. Tech. 19 (1): 37-50.

[Vaughan et. al., 1988] Vaughan, G., D. P. Wareing, L. Thomas, V. Mitev, 1988: Humidity measurements in the free troposphere using Raman backscatter, *Q. J. R. Meteor. Soc.*, **114**, 1471-1484.

[Wandinger, 1998] Wandinger, U., 1998: Experimental determination of the lidar overlap profile with Raman lidar Appl. Opt., 37, No. 3, 417-427.

[Wang et. al., 2003] Wang, J.,Carlson DJ, Parsons DB, Hock TF, Lauritsen D, Cole HL, Beierle K, Chamberlain E, 2003: Performance of operational radiosonde humidity sensors in direct comparison with a chilled mirror dew-point hygrometer and its climate implication Geophys. Res. Lett., 30, 16, 1860.

[Wang et. al., 2004] Wang, Z., D. N. Whiteman, B. B. Demoz, I. Veselovskii, 2004: A new way

to measure cirrus cloud ice water content by using ice Raman scatter with Raman lidar, Geophys. Res. Lett., Vol 31, L15101.

[Ware et. al., 2000] Ware RH, Fulker DW, Stein SA, Anderson DN, Avery SK, Clark RD, Droegemeier KK, Kuettner JP, Minster JB, Sorooshian S, 2000: SuomiNet: A real-time national GPS network for atmospheric research and education", Bull. Amer. Meteor. Soc. 81 (4): 677-694.

[Wechworth et. al., 2004] Weckworth T. M., IHOP, D. Parsons, S. Koch, J. Moore, M. LeMone, B. Demoz, C. Flamant, B. Geerts, J. Wang, W. Feltz, 2004: An Overview of the International H2O Project (IHOP_2002) and Some Preliminary Highlights", Bull. Amer. Meteor. Soc., Feb, 2004, 253-277.

[Whiteman et. al., 1992] Whiteman, D.N., S.H. Melfi, and R.A. Ferrare, 1992: Raman lidar system for the measurement of water vapor and aerosols in the earth's atmosphere", *Appl. Opt.*, **31**, No. 16, 3068-3082.

[Whiteman et. al., 1994] Whiteman, D. N., S. H. Melfi, R. A. Ferrare, K. D. Evans, 1993: Daytime Measurements of Water Vapor Mixing Ratio using Raman Scattering - Techniques and Assessment, 17th International Laser Radar Conference Abstracts of Papers, pp. 137-140.

[Whiteman and Melfi, 1999] Whiteman, D. N., S. H. Melfi, 1999: Cloud liquid water, mean droplet radius and number density measurements using a Raman lidar, *J. Geophys. Res.*, Vol 104 No. D24 December 27, 31411-31419.

[Whiteman et. al., 2001a] Whiteman, D. N., K. D. Evans, B. Demoz, D. O'C. Starr, E. Eloranta, D. Tobin, W. Feltz, G. J. Jedlovec, S. I. Gutman, G. K. Schwemmer, M. Cadirola, S. H. Melfi, F. J. Schmidlin, 2001: Raman lidar measurements of water vapor and cirrus clouds during the passage of hurricane Bonnie, *J. of Geophys. Res.*, 106, No. D6, 5211-5225.

[Whiteman et. al., 2001b] D. N. Whiteman, G. Schwemmer, T. Berkoff, H. Plotkin, L. Ramos-Izquierdo, G. Pappalardo, 2001: Performance modeling of an airborne Raman water vapor lidar, *Appl. Opt.*,**40**, No. 3, 375-390.

[Whiteman et. al., 2003a] Whiteman, David N, 2003a: Examination of the traditional Raman lidar technique. I. Evaluating the temperature-dependent lidar equations, Applied Optics, 42, No. 15, 2571-2592.

[Whiteman et. al., 2003b] Whiteman, David N., 2003b: Examination of the traditional Raman lidar technique. II. Evaluating the ratios for water vapor and aerosols, Applied Optics, 42, No. 15, 2593-2608.

[Whiteman et. al., 2005b] Whiteman, D. N., B. Demoz, P. Di Girolamo, J. Comer, I. Veselovskii, K. Evans, Z. Wang, M. Cadirola, K. Rush, D. Sabatino, G. Schwemmer, B. Gentry, S. H. Melfi, B. Mielke, D. Venable, T. Van Hove, E. Browell, R. Ferrare, S. Ismail, J. Wang, 2005: Raman Water Vapor Lidar Measurements During the International H_2O Project. II. Instrument Comparisons and Case Studies, this issue.

[Whiteman et. al., in preparation] Whiteman, D. N., B. Demoz, F. Russo, I. Veselovskii, Z. Wang, A. Gambacorta, K. Evans, L. Miloshevich, B. Lesht, H. Vömel, F. Schmidlin, P. Moore, A. Beebe, S.

Hannon, C. Barnet, Aqua validation using Raman Lidar and Radiosonde - the results of the AWEX field campaign, in preparation.